INTERNATIONAL SOCIETY FOR SOIL MECHANICS AND GEOTECHNICAL ENGINEERING

Non-linear finite-element analysis of axially loaded piles driven in chalk

K. Wen[1], S. Kontoe[2, 1], R. Jardine[1], T. Liu[3], L. Pan[1]

[1] Department of Civil and Environmental Engineering, Imperial College London, UK
[2] Department of Civil Engineering, University of Patras, Greece
[3] Department of Civil Engineering, University of Bristol, Bristol, UK

ABSTRACT: Driven piles are often employed to support onshore and offshore structures at low-density, porous weak carbonate chalk sites, which are encountered across Northern Europe and under the North and Baltic seas. Their efficient design is limited by uncertainties regarding their ultimate axial capacity and load-displacement behaviour. Intensive axial testing has been undertaken recently for the ALPACA Joint Industry Project on piles driven at a UK chalk site, in conjunction with comprehensive chalk characterisation studies. This paper presents PLAXIS-2D numerical simulations of such piles' axial loading behaviour. The simulation accounts for three distinct zones of chalk identified around the pile shafts after installation. These comprise a thin annular zone of de-structured, puttified, chalk and a second, thicker, annular zone of highly fractured chalk; both have different mechanical properties compared to the surrounding parent intact chalk mass. The FE analyses investigate how shaft resistance, axial capacity and load-displacement behaviour develop differently in compression and tension tests.

Keywords: Finite-element analysis; PLAXIS; axially loaded pile; chalk

1 INTRODUCTION

Research that combined advanced geotechnical laboratory, in-situ and large-scale field testing in conjunction with numerical modelling has delivered substantial benefits, including improved methods for designing monopiles driven to sustain lateral monotonic and cyclic loading at sand and clay sites (Byrne et al. 2020).

However, less attention has been given to designing jacket or monopiles driven in fractured and potentially brittle soft rocks like chalk, which is encountered frequently in piling projects across northern Europe (Mortimore, 2012). The increasing use of jacket structures to support offshore wind generators underscores the importance of developing reliable and cost-effective design guidance for axially loaded piles in such strata. The widely used CIRIA C574 guidance (Lord et al., 2002) offers only broad recommendations developed from a small and scattered dataset of field tests.

The ALPACA (Axial-Lateral Pile Analysis for Chalk Applying multi-scale field and laboratory testing) and ALPACA Plus Joint Industry Projects have sought to develop more representative, effective stress-based, design procedures through comprehensive field testing on 42 mostly instrumented piles driven at a well-characterised low-to-medium density chalk site, close to St. Nicholas-at-Wade (SNW), England. Jardine et al. (2023) summarise the research outcomes and update the axial capacity prediction procedures proposed by Buckley (2018) and Buckley et al. (2020), which addressed the important effects of driving and subsequent ageing effects in chalk.

Working in parallel, Wen et al. (2023) developed a load-transfer model to predict the monotonic axial pile load-displacement behaviour, accounting for the extreme radial property variations induced by pile driving and ageing in chalk. Meanwhile, Pedone et al. (2023) reported on the related ALPHA project (numerical Analysis of Laterally loaded Piles driven in cHAlk) which employed advanced constitutive models to reproduce the mechanical behaviour of SNW chalk and enable representative Finite Element analyses of the ALPACA programmes' unidirectional, monotonic lateral loading tests.

This paper reports finite element analyses which simulate the monotonic axial loading response of medium-scale open-ended driven piles observed in the ALPACA programme. A simplified procedure with the aid of ALPACA-SNW approach (Jardine et al. 2023) was utilised to explicitly account for the major effects on pile response of installation and ageing in-situ. This paper also investigates the difference in pile shaft capacities developed between tension and compression loading on identical piles.

2 PROBLEM DESCRIPTION

The analyses presented consider ALPACA piles LD07 and LD06, whose key parameters are given in Table 1. Both were driven through the Margate and underlying Seaford formations, which are structured, low-to-medium density, CIRIA Grade B2/B3 chalk, following Lord et al. (2002). Their characterisation through advanced in-situ and laboratory testing is described by Vinck et al. (2022).

Pairs of vertical Fibre Bragg (FBG) strain gauges were installed on opposing pile faces at ten levels over pile shafts, offering valuable insight into their axial load transfer mechanisms. A load cell and LVDT transducers monitored load-deflection behaviour at pile heads.

Table 1. Testing pile conditions at ALPACA research site

Parameters	Value
Outer diameter, D [m]	0.508
Wall thickness t_w [mm]	20.6
Pile embedment, L [m]	10.16
Age [days]	211
Groundwater level [m]	-6
Stick-up length [m]	1.5

Both piles were driven continuously to their full depths by hydraulic hammering and were allowed to rest for around 211 days prior to monotonic axial load-testing. As reported by Buckley (2018) and Jardine et al. (2023), pile driving creates an inner annulus of remoulded chalk putty around pile shafts (Zone A) as well as an outer annular zone where the chalk develops markedly greater fracturing (Zone B). The properties within these zones are distinct from those applying in the parent natural chalk mass (Zone C). The local radial effective stress developed along the pile shaft build greatly over the in-situ ageing period, which leads to significant pile capacity growth, or set-up, with final stresses that depend critically at any given depth on the local CPT resistance and relative normalised distance above the pile tip, h/R. These critical features should be accounted for in any representative numerical simulation of the piles' load-displacement behaviour.

3 NUMERICAL MODEL

3.1 Geometry and boundary conditions

The finite element analysis was performed using a 2D axisymmetric model with the software PLAXIS 2D V22 (Bentley Systems 2020). Figure 1 shows the model layout for the monotonic loading analysis, with the *y*-axis coinciding with the pile's axis. Horizontal and vertical fixities were applied at the bottom boundary of the model, which is set at a depth of 20 m ≈ 2L from the ground surface to avoid any boundary effects. The distant vertical boundary, at which orthogonal movements

were prevented, was located at a radius of 30 m ≈ 3L from the pile axis.

Following the field observations by Buckley (2018), the chalk domain was divided into various zones. The annular thickness of Zone A was assumed (from ground surface to the pile tip) equal to t_w, while the Zone B was $5t_w$ thick. A 0.5 m deep zone was also adopted below the pile tip with 'fractured chalk' properties to account for base installation effects. Following field observations, the piles' internal cores were treated as puttified chalk, even though its properties are slightly different to Zone A, as discussed subsequently.
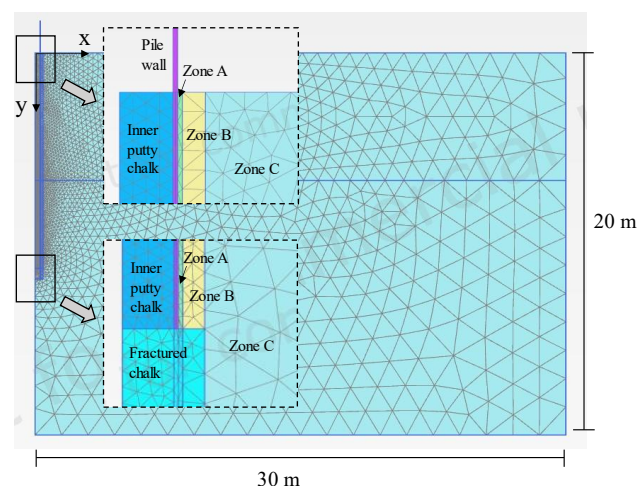

Figure 1 Geometry and mesh of the 2D finite element model

Figure 1 shows the discretisation of the chalk domain into 8052, 15-noded, triangular elements with 12 gauss points in each for accurate numerical integration. Finer discretisation was adopted in the area where stress concentrations are anticipated, particularly near pile shaft and base. The inner and outer pile-chalk interfaces were modelled using zero-thickness interface elements.

The tubular piles were treated as being elastic and were discretised into 1863 elements of the same type as employed in the chalk domain. The steel unit weight was 78.5 kN/m³, its Young's modulus was 210 GPa and its Poisson's ratio was 0.28.

3.2 Calculation phases

Three calculation phases were specified to capture the overall pile loading response during monotonic testing. Figure 2 shows a conceptual sketch covering the initialisation of the geostatic stress state within the chalk domain, the consideration of the pile installation and ageing effects, and finally, the application of monotonic pile loading. Given the relatively high in-situ permeability of chalk, all the numerical analyses were performed under drained conditions.

In the first phase, the chalk domain was treated as undamaged intact material, reproducing the initial in-situ stress state before pile penetration. The chalk's unit weight above and below the water table and the near-

hydrostatic pore pressure distribution were activated, based on the available site investigation measurements and a earth pressure coefficient pressure of $K_0 = 0.6$ after Vinck (2021).

The second phase was designated to achieve a realistic radial effective stress field in a simplified manner that attempts to reflect the major effects of pile installation and subsequent in-situ stress changes with time (pile ageing). Clusters representing the puttified chalk (inside and outside the pile wall) and fractured chalk (including the zone beneath the pile base) were activated before the cluster representing the pile was activated. The distribution of radial effective stress σ'_{rc} estimated from the long-term 'ALPACA-SNW' approach (Jardine et al. 2023) was imposed as an external stress boundary on the Zone A, approximated by a multilinear variation of stresses with depth. The in-situ geostatic vertical effective stress σ'_y was applied on the base. In order to prevent the collapse of the surrounding chalk, a horizontal fixity was imposed at the puttified chalk along the internal boundary with the pile. In the present study, the potential residual stress locked in piles during driving is neglected.

Although the efficiency of this simplified approach for predicting pile axial capacity has been noted by Said et al. (2010), it can not simultaneously reproduce the circumferential, radial and vertical effective stress state around driven piles, as measured for example around driven piles in sand by Jardine et al. (2013) and modelled by Yang et al. (2020).

Once the second calculation phase was completed, the imposed σ'_{rc} distribution, base pressure σ'_y and the relevant constraints along the inside puttified chalk were removed. In the meantime, any chalk displacements induced in the previous phase were reset to zero and the pile elements (weight and stiffness) were activated. This allowed the stress field condition adjacent to the pile shafts to be close to the ALPACA field measurements (although not presented herein for brevity) and ensures zero pile head displacement before imposing any external axial loads.

In the last phase, a displacement-controlled axial (tension/compression) load was imposed at the pile head (approximately 1.5 m above the ground surface) to simulate the piles' monotonic response.

3.3 Constitutive model and chalk properties

In the present research, a User-Defined Soil Model (UDSM) was implemeted with isotropic small strain stiffness and strain-softening Mohr-Coulomb failure criterion based on the non-local total strain E_d^{nl} (Taborda et al. 2016; Taborda et al. 2022a,b). This model allows chalk strength to retain peak values (c'_p and φ'_p) until $E_d^{nl} = E_{d,2}^{nl}$, which is followed by a linear reduction to residual strength (c'_f and φ'_f) corresponding to $E_d^{nl} = E_{d,3}^{nl}$. Note that the strain-softening failure criterion applies solely to the fractured chalk and intact chalk in this study, whereas for the puttified chalk aperfectly plastic failure criterion was adopted, as observed from labororay element testing (Vinck 2021, Pedone et al. 2023).

Pedone et al. (2023) have successfully ultilised similar constitutive models for reproducing the laterally loaded response of piles driven in chalk, in terms of lateral capacity and bending moment distributions. In their simulations, the initial shear modulus G_0 is assumed isotropic and independent of mean effective stress p', but reduces proportionally with the generalised deviatoric strain E_d. The meso- and macro-scale vertical fissures existed in the nactural chalk mass lead to the operational shear moduli approximately ¼ of the seismic CPT values following Vinck et al. (2022).

Table 2 lists the optimal set of constitutive parameters as adopted in the present study which are generally consistent with Pedone et al. (2023). G_{min} denotes the minimum shear stiffness, while a_o and b control the degradation rate of G_0. The peak and ultimate strength parameters c'_i, c'_f, φ'_i, φ'_f are calibrated against the experimental strength envelopes reported by Liu et al. (2022) and Pedone et al. (2023).
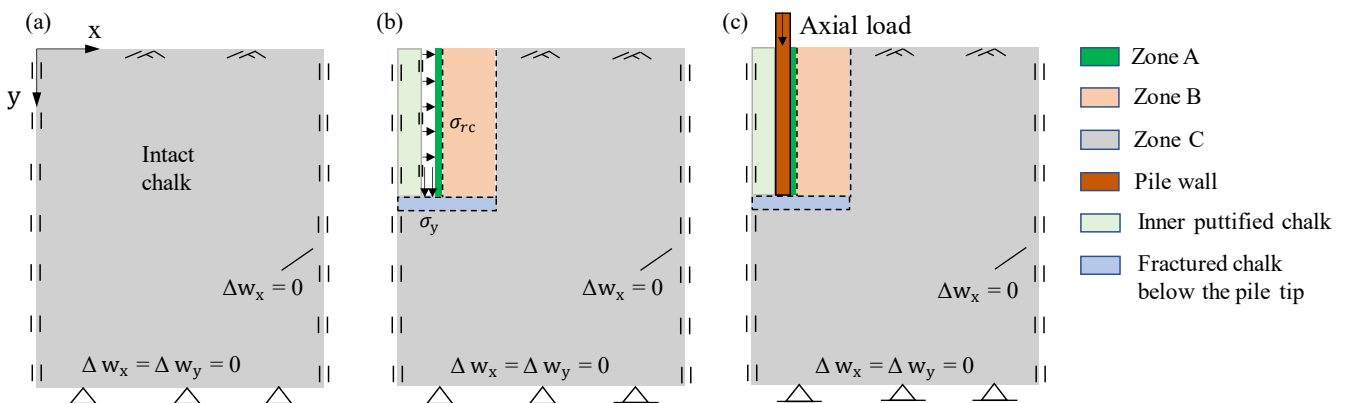

Figure 2. Three calculation phases in PLAXIS modelling; (a) the initialisation of the geostatic stress state within the chalk domain; (b) the consideration of the pile installation and ageing effects; (c) the application of monotonic loading

Although not present in Table 2, the inner puttified chalk plug and fractured chalk zone beneath pile base share the same strength properties as Zone A and Zone B respectively, while slight adjustments are made to their stiffness properties after conducting a parametric study. For example, G_{min} = 100 MPa is adopted for the inner puttified chalk while G_0 = 300 MPa for fractured chalk beneath pile base.

Table 2. Chalk parameters used in the numerical model

Parameters	Zone A	Zone B	Zone C
v	0.2	0.2	0.2
G_0 [MPa]	1000	50	500
G_{min} [MPa]	100	10	100
a_0	3.5E-5	1E-3	1E-3
b	1.3	4	4
c'_p [kPa]	3	159	747
c'_f [kPa]	3	5	5
φ'_p [°]	31.5	29	23.9
φ'_f [°]	31.5	31.5	31.5
ψ [°]	0	0	0
$E^{nl}_{d.2}$ [%]	-	0.5	0.5
$E^{nl}_{d.3}$ [%]	-	1.25	1.25

4 RESULTS AND DISCUSSION

4.1 Effects of pile-chalk interface properties

A parametric study was conducted by the Authors to explore the influence of interface properties on the simulation results of the LD06 tension pile. Given the adopted Coulomb failure criterion at the pile-chalk interface, the relevant strength parameters include the interface cohesion c_i and interface friction angle φ_i, the former taken as around 3 kPa in the present study (Vinck, 2021). Figure 3(a) assesses the sensitivity of the pile loading response to φ_i, with φ_i ranging from 19.0° to 29.0°. As expected, the higher the φ_i, the higher the ultimate capacities, although the variation of φ_i had relatively little impact on the stiffness evolution throughout loading. A φ_i value of 29° will be adopted, although this value is lower than measurements from long-term chalk/steel interface ring shear tests (Vinck, 2021). Figure 3 also shows the impact of the interface shear/normal stiffness parameters K_s and K_n respectively) on the pile load-displacement curves. In this case, adopting a combination of K_s = 3.0E5 kN/m³ and K_n = 2.5E6 kN/m³ (Pedone et al. 2023) led to the experimental load-displacement curve being reproduced satisfactorily at working loading levels, as discussed subsequently.

4.2 Comparison to experimental testing results

Figure 4 compares the numerically calculated and the experimental load-displacement curves for the tension loading test on LD06 pile. The prediction from a recently developed load transfer model (Wen et al. 2023) is also plotted for reference. Good agreement on the ultimate capacities is observed owing to the application of the radial effective stresses estimated by the ALPACA-SNW design guidance (Jardine et al. 2023). The numerical simulation produces a reasonable prediction of the initial stiffness at working loading levels (below approximately 30% of the ultimate loading capacity), although the pile head displacements are slight overestimated at high loading levels towards failure. The load transfer model proposed by Wen et al. (2023), however, offers better load-displacement predictions as failure approaches.

Figure 4 also shows the load-displacement prediction from a parallel numerical analysis without applying the external radial effective stress profile, while the remaining model conditions and chalk parameters were hold constant. Substantial underestimation of axial pile capacity underscores the significance of incorporating 'ALPACA-SNW' approach for adjusting the stress field around the pile shaft.

Figure 5 compares the calculated (solid lines) and measured axial force profiles for the LD06 pile. The axial force of the pile shows a broadly similar pattern at different levels of axial loads. A deflection point on the axial force profile is expected at the depth of the water table, due to the separate consideration of shaft resistances below and above the water table in the long-term 'ALPACA-SNW' approach (Jardine et al. 2023).
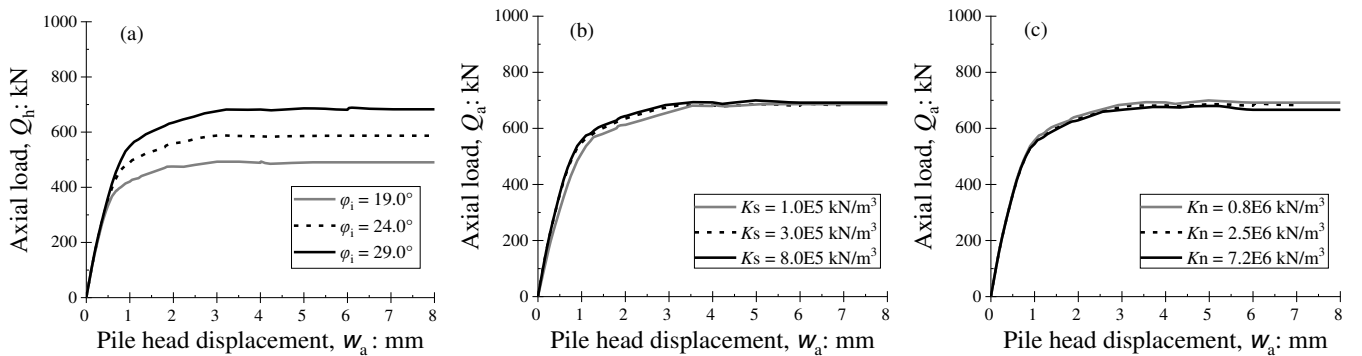

Figure 3. Influence of pile-chalk interface properties on pile head response; (a) interface friction angle φ_i; (b) interface shear stiffness K_s; (c) interface normal stiffness K_n

The axial force at the pile base is expected to be zero under tension loading. A good agreement with the experimental data is observed when the pile approaches failure (Q_a=693 kN), indicating its ability to reproduce reasonable axial force transfer at the ultimate state of the pile. At lower axial loads, although the match is reasonable at shallow depths, the numerical model consistently underestimates the axial pile forces below about 2.0 m depth. Differentiation with respect to depth of the axial force distribution leads to predictions for the mobilisation of local shaft resistances which confirm the deviations seen in some profiles at depths below about 2.0 m.
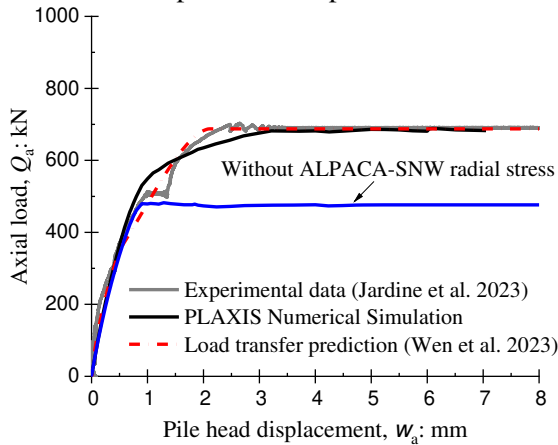

Figure 4 Comparison between numerical and experimental load-displacement curves for LD06 pile (tension loading)
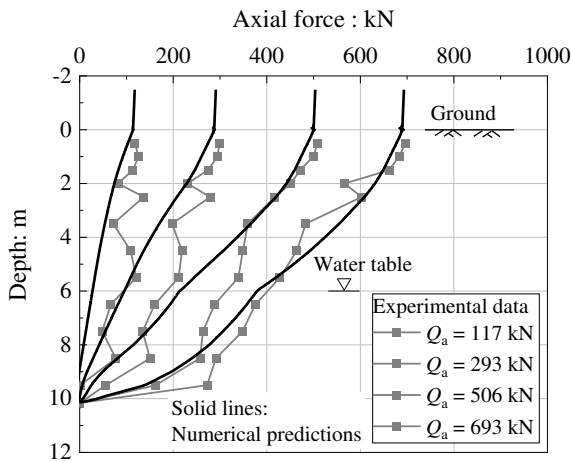

Figure 5 Comparison of the mobilised axial force distribution between calculated and experimental data

4.3 Distribution of shaft resistance from tension and compression tests

Jardine et al (2023) report that the loading direction has a crucial impact on driven pile shaft capacity in chalk. Figure 6 shows the predicted local shaft resistance profile from tension and compression piles LD06 and LD07, which are split into internal and external shaft resistances. The examined pile head displacement is 2 mm for both cases, at which the external pile shaft resistances were found to be fully mobilised. Note that the

negative sign is only used to distinguish tension and compression and it does not indicate the actual direction of shaft resistances.

As expected, the calculated external shaft resistances are broadly consistent with the ALPACA-SNW predictions. The compression case produces consistently higher external shaft resistance than the tension case, especially at shallow depths, indicting a more marked degree than the field tests. Integrating the shaft resistances over depth gives pile external capacities of around 671 kN and 581 kN in compression and tension cases respectively, leading to a compression/tension ratio of roughly 1.16, which can be interpreted as a Poisson's straining effect. The ratio remained fixed for $w_a > 2.0$ mm.

The internal shaft resistance builds up inside the compression pile LD07 pile to a far greater degree than in the LD06 tension pile, although internal resistances are negligible at levels more than 2D above the tip. Also plotted is the distribution of internal resistances at LD07 pile head displacement of 8.0 mm. This implies that the internal resistance in the vicinity of pile tip could increase considerably with further deflection due to plugging in the chalk. The computed ratio of compression to tension total shaft capacity (external + internal) increases to almost 2.5 after applying a displacement of $D/10$.

While this prediction matches well the ALPACA field data, it is not in agreement with other field evidence relating to the ratio of compression to tension shaft capacity. Vinck (2021) notes that a compression-to-tension shaft resistance ratio greater than 2 was found in field tests where the internal chalk plug had been removed by drilling. As noted earlier, the current study adopted a simplified initial stress procedure through a 'direct σ'_{rc} profile application' which does not explicitly consider the pre-loading stages caused by pile driving, or the circumferential and vertical stress distributions generated by later ageing. Its potential influence on pile loading behaviour requires further investigation.
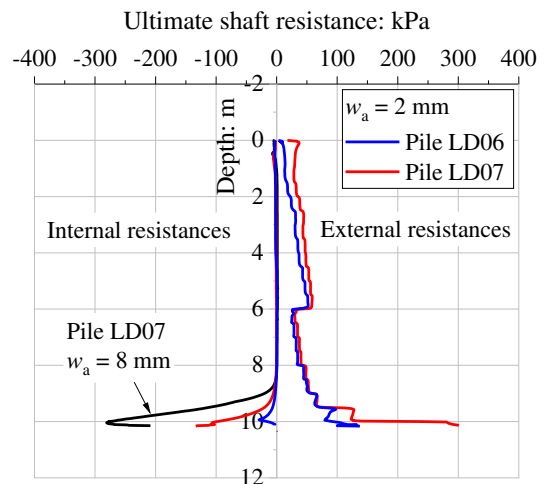

Figure 6 Ultimate shaft resistances derived from compression and tension tests

5 CONCLUSIONS

This paper compares finite element predictions for the monotonic axial loading response of piles driven in chalk with field measurements obtained from the ALPACA JIP. The numerical model accounted indirectly for pile installation and ageing effects by (i) applying 'ALPACA-SNW' predictions to initiate the radial effective stresses around the pile, (ii) simulating the chalk as a non-linear elastic material with strain-softening Mohr-Coulomb failure criterion based on the nonlocal total deviatoric strain. Four main conclusions follow:

1. Successful FE analyses rely on the modelling of pile installation effects through the division of the domain in puttified, fractured and intact chalk zones. Two additional zones, namely the inner puttified chalk zone and fractured chalk below pile tip, need special attention when modelling the response of compression loading pile.

2. Rigorous simulation of the pile-chalk interface plays a key role in the modelling of the axial pile loading response, in particular the interface strength.

3. Simulating the radial effective stresses acting on the pile shaft induced by driving and ageing critically influences the calculated ultimate pile capacity.

4. Applying the ALPACA-SNW design method profiles as external loads offered a simple approach that led to the computed pile shaft capacities varying with loading direction (tension or compression), as seen to a greater degree in the field tests. A relatively large proportion of the difference stems from the internal shaft resistance, which was far higher (near the tip) under compression loading. To further investigate this aspect, alternative simplified procedures for setting initial chalk stresses in the pre-monotonic loading stage are under investigation by the authors.

6 ACKNOWLEDGEMENTS

7 REFERENCES

Bentley Systems (2020) CONNECT Edition V21.00 PLAXIS 2D - Reference Manual.

Buckley, R. M. (2018). The axial behaviour of displacement piles in chalk. PhD Thesis, Imperial College London, London, UK.

Buckley, R. M., Jardine, R. J., Kontoe, S., Barbosa, P., Schroeder, F. C., (2020). Full-scale observations of dynamic and static axial responses of offshore piles driven in chalk and tills. Géotechnique 70 (8), 657-681.

Byrne, B. W., Houlsby, G. T., Burd, H. J., Gavin, K. G., Igoe, D. J. P., Jardine, R. J., Martin, C. M., McAdam, R. A., Potts, D. M., Taborda, D. M. G., Zdravković, L. (2020). PISA design model for monopiles for offshore wind turbines: application to a stiff glacial clay till. Géotechnique 70 (11), 1030-1047.

Jardine, R. J., Zhu, B. T., Foray, P., & Yang, Z. X. (2013). Interpretation of stress measurements made around closed-ended displacement piles in sand. Géotechnique, 63(8), 613-627

Jardine, R. J., Buckley, R. M., Liu, T., Andolfsson, T., Byrne, B., Kontoe, S., McAdam, R., Schranz, F., Vinck, K., (2023). The axial behaviour of piles driven in chalk. Géotechnique. doi: 10.1680/jgeot.22.00041

Lord J. A., Clayton, C. R. l. and Mortimore, R. N. (2002). Engineering in chalk, CIRIA, C574

Liu, T., Ahmadi-Naghadeh, R., Vinck, K., Jardine, R. J., Kontoe, S., Buckley, R. M., & Byrne, B. W. (2022). An experimental investigation into the behaviour of destructured chalk under cyclic loading. Géotechnique, ahead of print, doi: 10.1680/jgeot.21.00199.

Mortimore R. N. (2012). The 11th Glossop Lecture: Making sense of Chalk: a total-rock approach to its Engineering Geology. Q. J. Eng. Geol. Hydrogeol., 45, No.: 252-334

Pedone, G., Kontoe, S., Zdravković, L., Jardine, R. J., Vinck, K., & Liu, T. (2023). Numerical modelling of laterally loaded piles driven in low-to-medium density fractured chalk. Computers and Geotechnics, 156, doi: 10.1016/j.compgeo.2023.105252.

Said, I. D., De Gennaro, V., & Frank, R. (2009). Axisymmetric finite element analysis of pile loading tests. Computers and Geotechnics, 36(1-2), 6-19.

Taborda, D. M. G., Potts, D. M., & Zdravković, L. (2016). On the assessment of energy dissipated through hysteresis in finite element analysis. Computers and Geotechnics, 71, 180-194.

Taborda, DMG, Kontoe, S, Tsiampousi, A (2022a). IC MAGE Model 05 – Non-local strain-hardening/softening Mohr-Coulomb with isotropic small strain stiffness (Version 1.5). Zenodo. doi: 10.5281/zenodo.7198588

Taborda, DMG, Kontoe, S, Tsiampousi, A (2022b). IC MAGE UMIP –universal model interface for PLAXIS (Version 3.2). Zenodo. doi: 10.5281/zenodo.7129726

Vinck, K. (2021). Advanced geotechnical characterisation to support driven pile design at chalk sites. PhD thesis, Imperial College London, London, UK.

Vinck, K., Liu, T., Jardine R. J., Kontoe, S., Ahmadi-Naghadeh, R., Buckley, R. M., Byrne, B. W., Lawrance, J. A., McAdam, R. A., Schranz, F., 2022. Advanced in-situ and laboratory characterisation of the ALPACA chalk research site. Géotechnique, ahead of print, doi: 10.1680/jgeot.21.00197

Wen, K., Kontoe, S., Jardine R. J., Liu, T. (2023). An axial load transfer model for piles driven in chalk. Journal of Geotechnical and Geoenvironmental Engineering. (Minor Revision)

Yang, Z. X., Gao, Y. Y., Jardine, R. J., Guo, W. B., & Wang, D. (2020). Large deformation finite-element simulation of displacement-pile installation experiments in sand. Journal of Geotechnical and Geoenvironmental Engineering, 146(6), 04020044.